Excited-State Properties and Emission Spectra of Nonplanar Heterocyclic Helicenes

Karin Schmidt,[†] Sergio Brovelli,[‡] Veaceslav Coropceanu,[†] Jean-Luc Brédas,*[,†] Cristina Bazzini,[§] Tullio Caronna,[§] Riccardo Tubino,[‡] and Francesco Meinardi[‡]

School of Chemistry and Biochemistry and Center for Organic Photonics and Electronics, Georgia Institute of Technology, Atlanta, Georgia 30322-440, CNISM e Dipartimento di Scienza dei Materiali, Università di Milano Bicocca, Via Cozzi 53, I-20125 Milano, Italy, and Università di Bergamo, Dipartimento di Chimica Industriale della Facoltà di Ingegneria, Viale Marconi 5, I-24044 Dalmine (BG), Italy

Received: March 15, 2006; In Final Form: July 5, 2006

We discuss the electron-vibration coupling in mono-aza-[5]helicenes on the basis of a Franck−Condon analysis and density functional theory (DFT) calculations of the fluorescence and phosphorescence spectra measured in ethanol. The geometries of the initial states were obtained from time-dependent DFT (S_1) and unrestricted DFT (T_1) excited-state optimizations. In general, the position of the nitrogen atom has only a minor impact on the vibronic fine-structure in both absorption and emission. The shapes of the emission spectra from the lowest singlet and triplet states are found to be determined by contributions from multiple normal modes. The results of the calculations demonstrate how the interplay among these normal modes results in qualitatively and quantitatively different spectra for fluorescence and phosphorescence.

Introduction

Among the family of condensed aromatic molecules, [*n*]helicenes occupy a peculiar position as they consist of *n* fused six-membered rings that arrange in a nonplanar fashion due to steric hindrance. Thus, [*n*]helicenes combine the characteristics of a conjugated π-electron system with nonplanarity, which is known to increase spin−orbit coupling and to trigger intersystem crossing.[1−3] The enlarged spin−orbit coupling is accompanied by a molecular magnetic dipole moment[4,5] which is much larger than in planar aromatic molecules.

The emission properties have been discussed in the literature for [*n*]helicenes with $n = 4-7$ rings[1,6−12] and bisubstituted [5]helicenes[13] with a focus on intersystem crossing. The recently synthesized mono-aza-[5]helicene molecules[14] (see Figure 1) show a more efficient intersystem crossing than in the unsubstituted [5]helicene (H5);[15] in these molecules, a nitrogen atom has been introduced into the [5]helicene carbon backbone at positions 1−7, as illustrated in Figure 1, to form the mono-aza-derivatives 1-aza-H5 − 7-aza-H5. The interplay between phosphorescence and fluorescence is determined by several excitation transfer processes involving quasi-resonant states.[15] To provide an accurate description of such processes, in particular of spin−orbit coupling which is directly related to intersystem crossing, it is critical to determine the energetic positions of the relevant electronic states, including their vibronic sub-structure, and the vibronic coupling among them.

Even though the fluorescence and phosphorescence spectra of a variety of [*n*]helicenes have been reported,[1,16−19] to the best of our knowledge, no comprehensive theoretical investigation of the vibronic effects has been conducted yet. In the present work, our main goal is to provide a detailed understanding of the vibronic interactions and their impact on the fluorescence and phosphorescence properties of mono-aza-[5]helicenes. To access the lowest singlet and triplet states, S_1 and T_1, in a consistent way, we optimized their geometries at the density functional theory (DFT) B3LYP level. In the case of S_1, the time-dependent (TD) DFT methodology was used. Geometry determination at the TD-DFT level was recently demonstrated to reproduce very well the vibronic structures in the absorption spectra not only of many rigid molecules[20,21] but also of rather flexible pentathiophene oligomers.[21] Unrestricted DFT is a widespread method to optimize T_1 geometries; however, investigations of the vibrational fine-structure of phosphoresence spectra using DFT-based relaxed geometries are still scarce.[22]

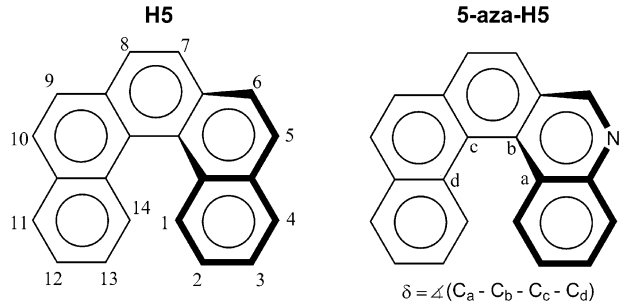

Figure 1. Chemical structure and atomic labels of [5]helicene and 5-aza-[5]helicene as a representative for the mono-aza-[5]helicenes.

Methodology

A. Experimental. Different strategies have been followed to prepare the [5]helicenes and all their possible monosubstituted aza-derivatives.[5] Solutions of these molecules in ethanol have been prepared at a concentration of 10^{-6} mol/L or lower.

The luminescence spectra have been collected with a Varian Eclipse Spectrofluorimeter at 77 K exciting the samples at 300 nm with a Xenon flash lamp. Fluorescence, in particular,

* To whom correspondence should be addressed. E-mail: jean-luc.bredas@chemistry.gatech.edu.
[†] Georgia Institute of Technology.
[‡] Università di Milano Bicocca.
[§] Università di Bergamo.

10.1021/jp0616258 CCC: $33.50
Published on Web 08/31/2006

is strongly affected by the presence of impurities. As pointed out by Grellmann et al.[23] and Lebon et al.,[5] the purification of [5]helicene requires a laborious chromatographic process. Synthesic precursors can remain and mainly consist of molecules with two or three fused rings. Such compounds are expected to show a strong fluorescence at energies beyond 3.4 eV. To limit the presence of such spurious signals, the fast emission from the singlet state has been recorded synchronously with the exciting flash lamp. On the contrary, phosphorescence has been collected asynchronously at 77 K with a delay time of 0.1 ms from the exciting flash and an integration time of 1 s. The emission bandwidth has always been held at 2.5 nm. Because several materials show a very small separation between the zero-phonon lines of absorption and fluorescence, measurements at different concentrations have been carried out to ensure that self-absorption does not affect the fluorescence signal. The degree of dilution ensured further that the emission spectra are not affected by aggregation.

In the case of H5 and 2-aza-H5, the aforementioned precursors could not be removed successfully from the material and their fluorescence signal is observed. This leads to a complicated convolution of the vibronic progressions related to both helicene and precursor emissions (not shown). For 2-aza-H5 in particular, we attribute the problem to the specific reaction route, which has a very small yield and has proven particularly difficult to provide purified 2-aza-H5. The presence of precursor remnants cannot be completely ruled out for 7-aza-H5.

B. Theoretical Background and Computational Details. It is useful to recall that the intensity of a radiative transition such as fluorescence and phosphorescence is described by the Einstein coefficient, A:

$$A = \frac{(E_1 - E_0)^3}{3\epsilon_0 \pi \hbar^4 c^3} |\vec{\mu}_{1\to 0}|^2 \tag{1}$$

Here, E_1 and E_0 are the energies of the excited and ground states and $\vec{\mu}_{1\to 0}$ is the corresponding transition dipole moment. In the framework of the Born−Oppenheimer (adiabatic) and Franck−Condon (FC) approximations, the transition dipole moment can be represented as a product of two factors that depend on electronic ($|e\rangle$) and vibrational ($|\nu\rangle$) degrees of freedom, respectively:

$$\vec{\mu}_{e^1\nu^1\to e^0\nu^0} = \vec{\mu}_{e^1\to e^0} \times \langle \nu^0(\boldsymbol{Q}^0)|\nu^1(\boldsymbol{Q}^1)\rangle \tag{2}$$

The shape of the emission bands, i.e., the *intensity distribution*, is governed by the overlap FCI(m, n) = $\langle \nu_n{}^0|\nu_m{}^1\rangle$ (FC integral) of the vibrational wave functions, where indices m and n denote the vibrational quantum numbers. The absolute intensity of the transition, i.e., the intensity integrated over the entire band, is solely determined by the electronic transition dipole moment.

In general, the sets $\boldsymbol{Q}^1$ and $\boldsymbol{Q}^0$ of normal modes obtained for two electronic states are different and related to each other by a linear transformation

$$\boldsymbol{Q}^1 = \boldsymbol{J}\,\boldsymbol{Q}^0 + \Delta\boldsymbol{Q} \tag{3}$$

in which matrix $\boldsymbol{J}$ is the so-called Duschinsky matrix and $\Delta\boldsymbol{Q}$ is the displacement between the equilibrium geometries of the considered electronic states. The calculations are considerably simplified in the parallel-mode approximation, which assumes that the normal coordinates of the electronic states of interest are identical.[24] In this case, the intensity distribution of a transition involving p vibrational modes reduces

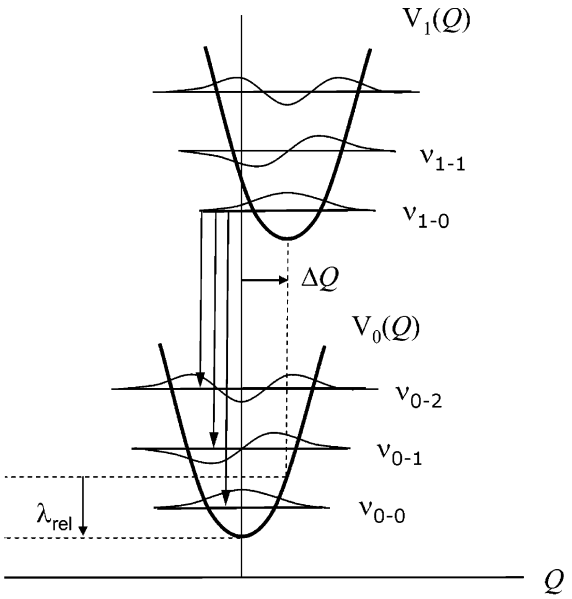

Figure 2. Schematic illustration of the potential energy surfaces in the displaced harmonic oscillator model, with indication of the λ_{rel} relaxation energy for emission (the vertical axis is energy).

to a product of FC integrals:

$$I(m_1, n_1, m_2, n_2, ..., m_p, n_p, E) = E^3 \times \delta(E - [E_{00} - \hbar \sum_i (n_i - m_i)\omega_i]) \times \prod_{i=1}^{p} \mathrm{FCI}(m_i, n_i)^2 \exp\left[-\frac{\hbar m_i \omega_i}{k_B T}\right] \tag{4}$$

where E_{00} is the (0−0) transition energy, m_i and n_i are the initial and final vibrational quantum numbers of mode ω_i, T is the temperature, and k_B is the Boltzmann constant.

For a given mode, the series of transitions $\nu_{1-n} \rightarrow \nu_{0-m}$ from the ground vibrational $n = 0$ level of the initial electronic state into the vibrational sublevels m of the final electronic state are schematically sketched in Figure 2. In the harmonic approximation (linear vibronic model), the FC integrals are expressed as:

$$\mathrm{FCI}(m, n)^2 = \exp(-S)\, S^{(n-m)} \frac{m!}{n!} [L_m^{(n-m)}(S)]^2 \tag{5}$$

Here, $L_n^{(\alpha)}(x)$ is a Laguerre polynomial and S denotes the Huang−Rhys factor. S provides a measure of the amount of energy contributed by a given mode to the overall relaxation energy λ_{rel}:

$$\lambda_{rel} = \sum_i \lambda_i = \sum_i \frac{k_i}{2} \Delta Q_i^2 = \sum_i \hbar\omega_i S_i \tag{6}$$

with

$$\lambda_i = \frac{k_i}{2} \Delta Q_i^2 \text{ and } S_i = \frac{\lambda_i}{\hbar\omega_i} \tag{7}$$

where ΔQ_i is the projection of $\Delta\boldsymbol{Q}$ along normal mode i and k_i is the corresponding force constant.

We performed geometry optimizations for the S_0 ground state and excited states S_1 and T_1 of all molecules, followed by calculations of the harmonic vibrational frequencies and normal modes. The calculations of S_0 and T_1 states were carried out at the restricted and unrestricted DFT levels, respectively. The

geometries in the S_1 states were obtained from TD-DFT[25−27] optimizations. In all cases, we used the B3LYP exchange-correlation functional[28] with a split valence SV(P) basis set, as implemented in the TURBOMOLE package.[29] For the sake of comparison, the geometries and vibrational modes were also computed using the semiempirical AM1[30] method in combination with a configuration interaction (AM1/CI) scheme, as implemented in the AMPAC program.[31]

The electronic transition energies were computed, on the basis of the (TD)DFT geometries: (i) in the adiabatic limit, which is defined as the energetic difference between the minima of the two potential surfaces (cf. Figure 2); and (ii) for the case of vertical transitions, in which we determined the energetic difference of the potential surfaces at the minimum geometry of the excited state with TD-DFT.

The Huang−Rhys factors S_i and the relaxation energies λ_i related to S_1-S_0 and T_1-S_0 transitions were computed using the DUSHIN program developed by Reimers.[32] The shapes of the emission spectra were simulated by calculating the Franck−Condon factors according to eq 5. In these calculations, the B3LYP vibrational frequencies have been scaled, according to literature, by a factor of 0.9613.[33] Because the vibronic structure in the spectra arises from transitions into the vibrational sublevels of the final state (see Figure 2), the analysis of fluorescence and phosphorescence has been carried out using the normal modes and Huang−Rhys factors of the ground-state S_0. The convolution of the resulting spectra was carried out with either Lorentzian functions of uniform width ($\sigma_{FWHM} = 0.03$ eV at 77 K and $\sigma_{FWHM} = 0.07$ eV at 298 K) in the case of fluorescence or Gaussian functions ($\sigma_{FWHM} = 0.01$ eV) for phosphorescence. The total reorganization energy λ_{rel} was estimated in two ways: (i) by summation over all individual normal-mode contributions λ_i according to eq 6; and (ii) by direct determination from the adiabatic potential surfaces, as schematically indicated by λ_{rel} in Figure 2 and described in detail elsewhere.[34,35] The onset E_{00} of the simulated spectra was chosen to match the maximum of the first peak of the simulated spectrum with the maximum of the (0−0) emission line found experimentally.

Results and Discussion

The calculated structural parameters characterizing the ground-state geometry, such as C−C and C−N bond lengths, bond angles, dihedral angles, and the helix pitch, are in excellent agreement with previously published values.[4,5,36] The dihedral angle δ (see Figure 1) is particularly sensitive to the nitrogen substitution site. As seen from Figure 4, the helices maintain a (DFT-optimized) δ value between 28 and 30°, which corresponds to a considerable deviation from planarity and matches the range $\delta_{exp} = 27-33°$ extracted from X-ray diffraction data.[5,14,37,38]

Table 1 collects the calculated totally symmetric modes for the H5 ground state (DFT-B3LYP) and the vibrations identified in IR, Raman, and highly resolved fluorescence spectra.[7] We have assigned our calculated modes to the experimentally observed vibrations on the basis of the vibrational energies and fluorescence intensities. The agreement between theory and experiment is very good, in particular for the intense fluorescence lines at 280, 1395, and 1428 cm^{-1}.

The relaxed geometries of the S_1 and T_1 states are notably different from the ground-state geometry in all molecules, see Figure 3. For 1-aza-H5, which is the only aza-H5 derivative whose nitrogen atom is placed in the inner periphery, the S_1 geometry could not be optimized with TD-DFT despite our efforts (such as changing initial geometries, the exchange-correlation functionals, or the quality of the basis set). It is not clear whether this failure has to be attributed to general shortcomings of our chosen methodology or whether the N1−H−C14 interaction (see Figure 1), which distinguishes 1-aza-H5 from all other molecules, generates a unique scenario in which the TD-DFT S_1 optimization fails.

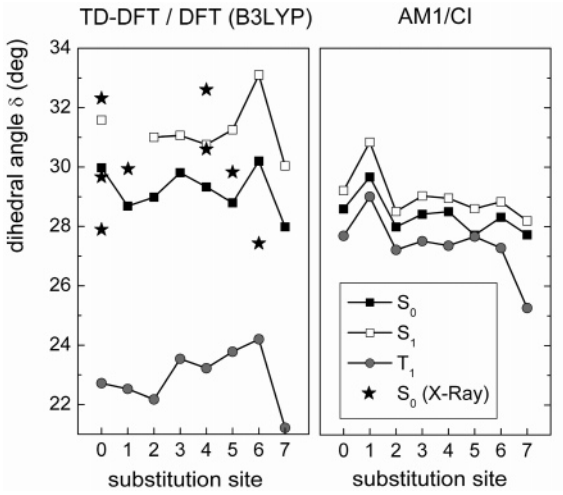

Figure 3. Evolution of the dihedral angle δ as a function of the substitution site, as determined by TD-DFT/DFT (left) and AM/CI (right) calculations. The dihedral angles found in the crystal structure are indicated with a star.[5,14,38,39] The multiple values shown for H5 and 4-aza-H5 correspond to nonequivalent molecules in the unit cell as well as to different crystal modifications.

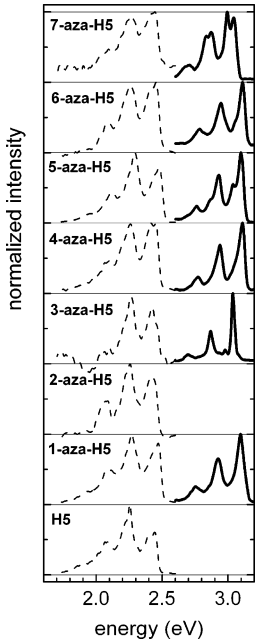

Figure 4. Normalized fluorescence (solid lines) and phosphorescence spectra (broken lines) of H5 and the mono-aza-H5 molecules in ethanol at 77 K.

The changes in molecular structure can be clearly tracked by considering: (i) the local modifications in C−C and C−N bonds; and (ii) the dihedral angle δ. Upon going from S_0 to S_1, the helices tend to open up, i.e., δ increases with respect to the S_0 geometry. On the other hand, going from S_0 to T_1 decreases δ. These trends are obtained with both DFT(B3LYP) and AM1 calculations and TD-DFT (B3LYP) and AM1/CI calculations, respectively (Figure 3). The opening or flattening of the helices during relaxation is expected to involve vibrations whose

TABLE 1: Scaled Frequencies and Huang−Rhys Factors *S* of the $S_0 \rightarrow S_1$ Transition for the Totally Symmetric Normal Modes of [5]Helicene Obtained for the S_0 Ground State (DFT/B3LYP)[a]

DFT-B3LYP		fluorescence		IR	Raman
$0.9613 \times \hbar\omega$ (cm^{-1})	*S*	$\hbar\omega$ (cm^{-1})		$\hbar\omega$ (cm^{-1})	$\hbar\omega$ (cm^{-1})
87	0.468	107	w		
165	0.058	180	m	180	180
241	0.135	234	vw	230	230
269	0.233	280	s	280	275
407	0.066	420	m	410	415
440	0.009	465	w	460	460
525	0.007	510	w	512	535
563	0.049	602	w	598	
654	0.023				665
841					*855*
906	0.010	930	vw	938	
		1285	m		
1322	0.026	1328	vw	1320	
1341	0.244	1395	s	1390	1380
1361	0.150	1428	s	1418	
1600	0.049				
1614	0.011				

[a] The vibrations identified in the 4.2 K fluorescence spectrum (*n*-pentane matrix) and the vibrations observed in IR and Raman spectra according to ref 7 are shown for comparison and are assigned tentatively. To associate the Raman mode found at 855 cm^{-1}, the frequency of an antisymmetric mode (italics) is also shown (w = weak, m = medium, s = strong, v = very).

elongation pattern is altering the molecular height. Thus, we can anticipate that normal vibration modes that affect the molecular height (i.e., correspond to a wagging motion) are strongly coupled to S_0-S_1 and S_0-T_1 absorption and emission processes.

Although the general trends are rather similar, AM1/CI geometries for S_1 and T_1 deviate much less from the S_0 geometry than what is predicted by (TD-)DFT. Whereas in DFT the flattening ($\Delta\delta \approx 7°$) in T_1 is much more pronounced than the opening ($\Delta\delta \approx 7°$) into S_1 in TD-DFT, the amount by which the helix pitch is altered with AM1/CI is much smaller ($\Delta\delta \approx 1°$) (Figure 3), whatever excited-state considered. The evolution of δ as a function of the N position differs somewhat from the DFT-results with 1-aza-H5 being the most obvious instance. Furthermore, the local changes of the AM1/CI bond lengths are smaller than those seen in (TD-)DFT. We will come back later to a discussion of the relative merits of the (TD-)DFT and AM1/CI optimized structures.

Upon relaxation from the initial ground-state geometry into the optimized S_1 geometry, the electronic nature of the lowest excited states is kept: In all molecules, S_1 mainly involves two configurations that correspond to HOMO-1 to LUMO and HOMO to LUMO+1 transitions; S_2 consists of the two configurations associated to HOMO to LUMO and HOMO-1 to LUMO+1 transitions, in agreement with previous findings from (ground-state) CNDO/S calculations.[39] The lowest triplet state T_1 is represented by a single HOMO to LUMO configuration according to the TD-DFT calculations.

The transition energies extracted from the experimental spectra (Figure 4) are shown in comparison to the calculated energies in Table 2. It is clear from experiment that the positions of the fluorescent (2.99−3.11 eV) and phosphorescent (2.42−2.46 eV) states hardly fluctuate with the N location. The positions of the (0−0)-phonon lines can be roughly compared to the calculated adiabatic transition energies (i.e., the energy difference between the minima of the adiabatic potential surfaces of the excited and ground electronic states), although in doing

TABLE 2: Transition Energies $S_1 \rightarrow S_0$ and $T_1 \rightarrow S_0$, Given by the Positions of the (0−0)-Lines, from the Emission Spectra (77 K) in Ethanol in Comparison to the Calculated Adiabatic and Vertical (TD-)DFT Transition Energies

	singlet E_{S_1} (eV)			triplet E_{T_1} (eV)		
		TD-DFT			TD-DFT	
compound	exp.	adiab.	vert.	exp.	adiab.	vert.
H5	−	3.24	3.12	2.45	2.19	1.76
1-aza-H5	3.10	−	−	2.48	2.29	1.80
2-aza-H5	−	3.25	3.12	2.42	2.19	1.78
3-aza-H5	3.04	3.22	3.09	2.47	2.20	1.78
4-aza-H5	3.11	3.23	3.10	2.45	2.21	1.78
5-aza-H5	3.10	3.28	3.15	2.47	2.24	1.81
6-aza-H5	3.11	3.27	3.14	2.45	2.21	1.76
7-aza-H5	3.04	3.21	3.07	2.44	2.21	1.79

TABLE 3: Total Relaxation Energy λ_{rel} of the $T_1 \rightarrow S_0$ Transition of Mono-aza-[5]helicenes Obtained from Normal-Mode (NM) Calculations and from the Potential Surfaces (PS)

compound	λ_{rel} (NM)/ (eV)	λ_{rel} (PS)/ (eV)
H5	0.447	0.426
1-aza-H5	0.438	0.417
2-aza-H5	0.438	0.419
3-aza-H5	0.442	0.420
4-aza-H5	0.448	0.424
5-aza-H5	0.462	0.435
6-aza-H5	0.479	0.454
7-aza-H5	0.441	0.421

so we neglect solvent effects, an additional stabilization due to the coupling to intramolecular low-frequency vibrations, and the difference in the zero-point energies. The TD-DFT estimates of the adiabatic $S_1 \rightarrow S_0$ energies (TD-DFT: $E^{ad}_{S_1} = 3.21-3.28$ eV) as well as the adiabatic $T_1 \rightarrow S_0$ energies derived from DFT calculations (DFT: $E^{ad}_{T_1} = 2.53-2.58$ eV) are in good agreement with experimental data (cf. Table 2).

A. Phosphorescence. The radiative transition between the lowest triplet state and the ground state gives rise to a $T_1 \rightarrow S_0$ phosphorescence signal. The phosphorescence intensities recorded for H5 and the mono-aza-helicenes vary strongly as a function of the position of the nitrogen atom.[15] Compared to the phosphorescence signal of H5, the presence of the nitrogen atom does not significantly affect the line shape, which is similar throughout the series (Figure 4). In general, the (0−1) and (0−0) lines are of similar intensity with their intensity ratio slightly fluctuating with altering the N-site. While the (0−1) line dominates the spectrum for H5, the (0−0) line gains intensity upon introduction of N and becomes slightly stronger than (0−1) in 6- and 7-aza-H5.

The relaxation energies λ_{rel} related to the $T_1 \rightarrow S_0$ transition obtained from the potential energy surfaces are listed in Table 3 for all molecules. In agreement with experiment, the replacement of a carbon atom with a nitrogen atom upon going from H5 to a mono-aza-H5 leads only to a minor variation in λ_{rel}. We also evaluated the partition of the relaxation energies into the contributions of each normal mode according to eqs 6 and 7. The relaxation energies obtained from the adiabatic potential surface calculations and the normal-mode approach are in excellent mutual agreement (see Table 3). The vibration coupling constants (Huang−Rhys factors), determined for each of the molecules, are not significantly altered when changing the position of the nitrogen atom in the helicene. In particular, the interactions with high-energy modes that are responsible for the main contribution to λ_{rel} remain nearly unaffected.

As an illustrative example of normal-mode calculations, the vibrational couplings derived for H5 are given in Table 4. The

TABLE 4: DFT/B3LYP Estimates of Frequencies and Huang−Rhys Factors Related to the $T_1 \rightarrow S_0$ Transition in H5

$\hbar\omega$ (cm^{-1})	S	$\hbar\omega$ (cm^{-1})	S	$\hbar\omega$ (cm^{-1})	S	$\hbar\omega$ (cm^{-1})	S
65	0.132	680	0.018	1065	0.001	1472	0.043
91	1.358	727	0.019	1096	0.005	1528	0.005
172	1.214	753	0.006	1163	0.005	1571	0.181
251	0.002	775	0.019	1167	0.095	1642	0.725
280	1.136	838	0.016	1175	0.030	1664	0.030
344	0.005	865	$<10^{-3}$	1217	0.003	1679	0.022
423	0.199	872	0.001	1228	$<10^{-3}$	3162	$<10^{-3}$
458	0.060	910	0.008	1250	0.065	3164	$<10^{-3}$
473	0.351	942	0.038	1298	0.004	3174	$<10^{-3}$
484	0.016	984	0.002	1375	0.111	3181	$<10^{-3}$
546	0.005	991	0.002	1395	0.231	3184	$<10^{-3}$
586	0.094	1006	0.006	1416	0.090	3189	$<10^{-3}$
621	0.005	1020	$<10^{-3}$	1454	$<10^{-3}$	3223	$<10^{-3}$

relaxation energy is dominated by high-energy vibrations in the range 1200−1700 cm^{-1}. The relaxation contribution associated to the contribution of these modes accounts for more than 60% of the overall relaxation energy λ_{rel}. The vibrational modes at 1642 and 1395 cm^{-1} that yield the largest Huang−Rhys factors in the high-frequency range are illustrated in Figure 5. These vibrations correspond to stretching of C−C bonds mainly located either in the terminal rings (1642 cm^{-1} mode) or in the central ring (1395 cm^{-1} mode) of the molecule. As seen from Table 4, there is also a strong coupling with low-energy vibrations below 300 cm^{-1}. Each of these low-frequency modes correspond to a flip-flop motion, illustrated for the modes at 91 and 280 cm^{-1} in Figure 5. Despite the fact that they contribute only moderately to the relaxation energy due to their small frequency, these modes possess large Huang−Rhys factors and therefore have an important effect on the phosphorescence spectrum.

The results of the normal-mode analysis have been further exploited to simulate the shape of the phosphorescence spectra. All vibrational modes with Huang Rhys factors $S \geq 0.01$ have been taken into account, because modes with $S < 0.01$ essentially do not contribute. The results of the simulations for 1-aza-H5, 5-aza-H5, and 6-aza-H5 are shown in Figure 6. The simulated spectra reproduce well the measured spectra both in terms of energy progression as well as intensity distribution**.** The shape of the spectra is dominated by the coupling with several modes in the 1600 cm^{-1} region. The energy spacings between these vibrations are smaller than the inhomogeneous broadening and in addition (as shown in Table 7) the modes are subject to significant Duschinsky mixing. As a consequence, their individual contributions to the spectra cannot be resolved and their collective action rather resembles the effect of a single effective mode with a Huang−Rhys factor close to unity. This gives rise to (0−0) and (0−1) transitions of approximately the same intensity. However, a second group of strongly coupled modes at 1400 cm^{-1} is also present, and actually leads to a further increase in the relative intensity of the (0−1) transition with respect to the (0−0) peak. This pattern is shared by all simulated spectra, including the limiting cases posed by 6- and 7-aza-H5 (cf. Figure 6) whose (0−0) line is actually slightly more intense with respect to (0−1) in experiment.

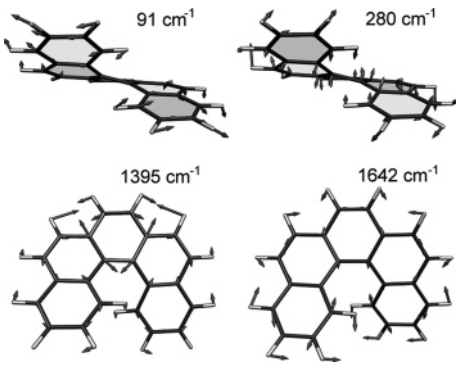

Figure 5. Elongation patterns of representative normal modes of H5.

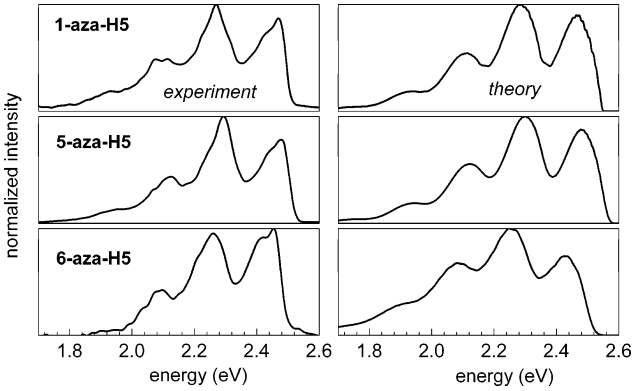

Figure 6. Normalized phosphorescence spectra (left) of mono-aza-[5]helicenes (ethanol, $T = 77$ K) in comparison to the simulated phosphorescence spectra (right). The onset of the simulated spectra is chosen to correspond to experimental onset. The theoretical spectra were convoluted with Gaussian functions of width $\sigma_{FWHM} = 0.015$ eV.

TABLE 5: Total Relaxation Energy λ_{rel} of the $S_1 \rightarrow S_0$ Transition of Mono-aza-[5]helicenes Obtained from Normal-Mode (NM) Calculations and from the Potential Surfaces (PS)

compound	λ_{rel} (NM)/ (eV)	λ_{rel} (PS)/ (eV)
H5	0.129	0.123
1-aza-H5	−	−
2-aza-H5	0.129	0.123
3-aza-H5	0.139	0.133
4-aza-H5	0.137	0.131
5-aza-H5	0.137	0.130
6-aza-H5	0.136	0.130
7-aza-H5	0.145	0.140

TABLE 6: DFT/B3LYP Estimates of Frequencies and Huang−Rhys Factors Related to the $S_1 \rightarrow S_0$ Transition in H5

$\hbar\omega$ (cm^{-1})	S	$\hbar\omega$ (cm^{-1})	S	$\hbar\omega$ (cm^{-1})	S	$\hbar\omega$ (cm^{-1})	S
65	0.097	680	0.023	1065	0.001	1472	$<10^{-3}$
91	0.468	727	0.001	1096	$<10^{-3}$	1528	0.020
172	0.058	753	0.005	1163	0.001	1571	0.001
251	0.135	775	$<10^{-3}$	1167	0.001	1642	0.001
280	0.233	838	0.002	1175	0.002	1664	0.049
344	0.007	865	0.001	1217	$<10^{-3}$	1679	0.011
423	0.066	872	$<10^{-3}$	1228	0.012	3162	$<10^{-3}$
458	0.009	910	0.002	1250	0.003	3164	$<10^{-3}$
473	$<10^{-3}$	942	0.010	1298	0.003	3174	$<10^{-3}$
484	0.001	984	0.001	1375	0.026	3184	$<10^{-3}$
546	0.007	991	0.001	1395	0.244	3181	$<10^{-3}$
586	0.049	1006	$<10^{-3}$	1416	0.150	3189	$<10^{-3}$
621	$<10^{-3}$	1020	0.002	1454	0.017	3223	$<10^{-3}$

These modes are also responsible for the systematic decrease in energy separation between the main peaks as we move away from the (0−0) origin of the spectra. Along with low-frequency modes, they are also contributing to the asymmetry and broadening of the main peaks. A similar behavior, where several modes contribute to a vibrational fine-structure that appears like a single vibronic progression, has been documented, e.g., for ultraviolet photoelectron spectroscopy (UPS) spectra of oligoacenes.[35]

TABLE 7: Excerpt of the Duschinsky Matrix *J* Coupling the Symmetric Modes of S_0 and T_1 in [5]Helicene[a]

I		*II*		*III*		*IV*	
91 cm^{-1}		280 cm^{-1}		1395 cm^{-1}		1642 cm^{-1}	
$\hbar\omega_i$	$J_{I,i}$	$\hbar\omega_i$	$J_{II,i}$	$\hbar\omega_i$	$J_{III,i}$	$\hbar\omega_i$	$J_{IV,i}$
92	0.729	264	−0.854	1380	−0.609	1685	−0.785
93	0.662	258	0.424	1390	−0.551	1620	−0.562
835	0.304	352	0.154	1507	0.277	1490	−0.125
264	0.152	469	−0.084	1490	0.232	1523	0.103
258	0.134	175	−0.078	1449	0.187	1449	−0.100
488	0.125	1507	−0.071	1269	−0.173	1630	−0.084
902	0.121	1685	0.061	1581	−0.154	1269	−0.082

[a] Shown are the coefficients $J_{k,i}$ with which the normal modes $\hbar\omega_i$ of T_1 contribute to the vibrational normal modes $\hbar\omega_k$ of the S_0 shown in Figure 5.

Because the relaxation energies computed for all mono-aza-helicenes hardly change with the nitrogen position, the simulated spectra are also almost unaffected by the actual nitrogen position. The experimental differences are, in fact, more pronounced (see Figure 4). We attribute this discrepancy to the approximations used in our approach and the neglect of solvent effects. This suggests that a simulation based on multidimensional Franck−Condon factors and accounting for Duschinsky mixing, as well as the inclusion of interactions with the solvent into the model, might further improve the agreement between theoretical and experimental spectra.

Finally, we investigated to which extent AM1/CI geometry-based simulations are capable to predict differences between the N-sites. Upon relaxation from T_1 into S_0, both the C−C(/N) bond lengths as well as the dihedral angle δ (shown in Figure 3) are much less modified by AM1/CI than by DFT. Consequently, the vibrational coupling between modes in the 1400 and 1600 cm^{-1} range is much smaller than for DFT, and the coupling to low-frequency modes is essentially absent. The phosphorescence spectra simulated on that basis are narrow and dominated by an effective (0−0) transition. Because this picture contradicts the experimental observation, we conclude the DFT-calculated geometries are clearly superior to the AM1/CI optimized structures, at least for the molecules considered in this work.

B. Fluorescence. The relaxation energies λ_{rel} related to the $S_1 \rightarrow S_0$ transition obtained from potential energy surfaces and normal-mode calculations are listed in Table 5. Both direct methods yield consistent total relaxation energies λ_{rel} of ca. 130 meV. The introduction of a nitrogen atom is predicted to increase slightly the relaxation energies. The relaxation energy is hardly sensitive to the position of the heteroatom in the molecule (variations in the range 123−133 meV) except for 7-aza-H5 in which λ_{rel} adopts its largest value in the series (140 meV). The λ_{rel} values are a factor of 3 smaller than the relaxation energies for the $T_1 \rightarrow S_0$ transition. As an example, the normal modes and Huang−Rhys factors calculated for H5 are reported in Table 6; the Huang−Rhys factors found in H5 from the theoretical analysis compare favorably with the intensity of vibrations identified in highly resolved low-temperature fluorescence spectra,[7] in particular for the most intense lines.

The fluorescence portion of the emission spectra is shown for representative molecules in Figure 7 in comparison to the results of the theoretical simulations. Because eq 4 only takes into account the temperature-dependent homogeneous broadening, the simulated spectra for 77 and 298 K have been convoluted uniformly for all molecules with Lorentzians of 0.03 and 0.07 eV FWHM, respectively, to account for the inhomogeneous broadening as well. The main progression of fluorescence is exclusively determined by a high-frequency mode at ca. 1400 cm^{-1} that possesses the largest Huang−Rhys factor. The Huang−Rhys factors found for the low-frequency modes are considerably smaller than for the T_1-S_0 transition. Thus, the lines in the fluorescence spectra are intrinsically narrower than in phosphorescence. The general trends seen in the emission spectra at 77 K confirm this finding (Figure 4). The line spacings in the simulated spectra match well the experimental ones, while the intensity distributions cannot be perfectly reproduced. Additionally, the splitting of the (0−0) line observed in the 7-aza-H5 spectrum is absent in our simulations. The calculated intensities of the (0−1) and (0−2) transitions are smaller with respect to the (0−0) peak than in experiment. This underestimation might be directly related to the insufficient amount of exact Hartree−Fock exchange in the hybrid B3LYP functional[21] or possibly caused by a nonadiabatic coupling between rather closely spaced electronic states. According to our TD-DFT calculations, the lowest two singlet states S_1 and S_2 are separated by less than 0.3 eV and are, thus, sufficiently close in energy to be coupled nonadiabatically. Another possible reason is the neglect of the solvent in our calculations. The neglect of the Duschinsky mixing can be ruled out as a possible reason for this discrepancy, because the modes superimposed by the Duschinsky matrix can be considered degenerate and, thus, do not give rise to further transitions at different energies. In addition, inharmonic contributions should not play a role, because the estimates for the total relaxation energies are mutually consistent, be them determined from the potential surfaces or from the vibrational analysis in the harmonic approximation (Table 5). In the particular case of 7-aza-H5, the apparent splitting in the (0−0) line can be explained neither within the framework of our model, nor by considering additional effects that were mentioned above. Rather, the overall shape of the spectrum is reminiscent of the superposition of the luminescence from two inequivalent emitting species, one of which possibly being a contaminant. The experimental fluorescence spectra reported for [5]helicene in the literature differ considerably in shape and, thus, have to be considered with care. Brown et al.[16] and Grellmann et al.[23] observed, for instance, a very different intensity distribution in the fluorescence signal measured in different solvents, even though the main progression is given by a high-frequency mode around 1400 cm^{-1} in both experiments, as found in our investigation.

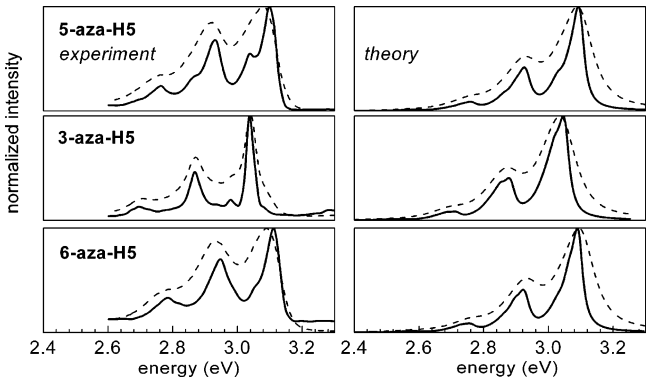

Figure 7. Normalized fluorescence spectra (left) of mono-aza-[5]helicenes (ethanol, $T = 77$ K solid, $T = 298$ K dashed) in comparison to the simulated (right) fluorescence spectra. The onset of the simulated spectra is chosen to correspond to experimental onset. The theoretical spectra were convoluted with Lorentzian functions of width $\sigma_{FWHM} = 0.03$ eV for the 77 K spectra (solid) and $\sigma_{FWHM} = 0.07$ eV for the 298 K spectra (dashed).

Conclusions

[5]Helicene and its mono-aza-derivatives share a characteristic emission pattern. There is a marked difference between the spectral shape of the $S_1 \rightarrow S_0$ transitions and that of the $T_1 \rightarrow S_0$ transitions. The theoretical simulation demonstrates that this difference arises from the vibronic coupling which is distinctively different for the $S_1 \rightarrow S_0$ and $T_1 \rightarrow S_0$ transitions. In phosphorescence, the combination of two high-frequency modes of ca. 1400 and 1600 cm^{-1} determines the main progression. In contrast, the vibronic structure observed in fluorescence is predominantly due to the progression of a single mode at ca. 1400 cm^{-1} (which is the same mode that partially contributes to the vibronic progression in phosphorescence). The peaks arising from the high-frequency modes in phosphorescence are broader than in fluorescence. We attribute this finding to the stronger coupling to the low-frequency modes between 50 and 300 cm^{-1} in the $T_1 \rightarrow S_0$ transition than in the $S_1 \rightarrow S_0$ transition; this gives rise to a larger homogeneous broadening in phosphorescence than in fluorescence.

Our theoretical calculations, which rely on DFT in the case of phosphorescence and TD-DFT/DFT for fluorescence, reproduce the energetic positions and asymmetry of the line-shape of the experimental spectra very well. The intensity distribution predicted for $T_1 \rightarrow S_0$ is in excellent agreement with the phosphorescence signal. In the case of fluorescence, however, our method (which combines TD-DFT for the S_1 geometry and DFT for the S_0 geometry) systematically underestimates the Huang−Rhys factor of the main mode.

Our theoretical investigation of the electronic structure of the states involved as well as the electron-vibration coupling between them reveals almost no sensitivity to the nitrogen position, which explains the shape conservation in the emission spectra throughout the series of mono-aza-[5]helicenes. In addition, the energy onset of emission is hardly affected by the presence and position of the N-atom. We attribute this finding to the $\pi-\pi^*$ character of the transitions involving the S_0, S_1, and T_1 states; therefore, these states do not differ significantly from the corresponding states (and vibrations) in [5]helicene.

The phosphorescence-to-fluorescence ratio among the mono-aza-[5]helicenes was found to vary strongly with the nitrogen position. With the present work, we can exclude vibronic coupling, which is independent from the location of the nitrogen atom within the carbon backbone, as a possible origin. Rather, spin−orbit coupling must give rise to the strong dependence of the intersystem crossing on the nitrogen-site; the investigation of this process in mono-aza-[5]helicenes is in progress.[15]

Acknowledgment. We are indebted to J. Reimers for most kindly providing the DUSHIN program. The work at the Georgia Institute of Technology was supported by the National Science Foundation (Grant CHE-0342321, CRIF 04-43564) and the Office of Naval Research.

References and Notes

(1) Sapir, M.; Vander Donckt, E. *Chem. Phys. Lett.* **1975**, *36*, 108−110.

(2) Beljonne, D.; Shuai, Z.; Pourtois, G.; Brédas, J. L. *J. Phys. Chem. A* **2001**, *105*, 3899−3907.

(3) Nijegorodov, N. I.; Downey, W. S. *J. Phys. Chem.* **1994**, *98*, 5639−5643.

(4) Furche, F.; Ahlrichs, R.; Wachsmann, C.; Weber, E.; Sobanski, A.; Vögtle, F.; Grimme, S. *J. Am. Chem. Soc.* **2000**, *122*, 1717−1724.

(5) Lebon, F.; Longhi, G.; Gangemi, F.; Abbate, S.; Priess, J.; Juza, M.; Bazzini, C.; Caronna, T.; Mele, A. *J. Phys. Chem. A* **2004**, *108*, 11752−11761.

(6) Palewska, K.; Ruziewicz, Z.; Chojnacki, H. *Chem. Phys.* **1992**, *161*, 437−445.

(7) Palewska, K.; Chojnacki, H. *J. Mol. Struct.* **2002**, *611*, 23−32.

(8) Palewska, K.; Chojnacki, H. *Mol. Cryst. Liq. Cryst.* **1993**, *229*, 31−36.

(9) O′Dwyer, M. F.; Ashraf El-Bayoumi, M.; Strickler, J. *J. Chem. Phys.* **1962**, *36*, 1395−1396.

(10) (a) Clar, E.; Zander, M. *Aromatische Kohlenwasserstoffe* **1956**, *89*, 749−762. (b) Clar, E. *Polycyclic Hydrocarbons*; Academic Press: London, 1964; pp 277−280.

(11) Kim, S. S.; Weissman, S. I. *J. Am. Chem. Soc.* **1969**, *101*, 5863−5864.

(12) Weigang, O. E., Jr.; Turner, J. A.; Trouard, P. A. *J. Chem. Phys.* **1966**, *45*, 1126−1134.

(13) Caronna, T.; Gabbiadini, S.; Mele, A.; Recupero, F. *Helv. Chim. Acta* **2002**, *85*, 1−8.

(14) Bazzini, C.; Brovelli, S.; Caronna, T.; Gambarotti, C.; Giannone, M.; Macchi, P.; Meinardi, F.; Mele, A.; Panzeri, W.; Recupero, F.; Sironi, A.; Tubino, R. *Eur. J. Org. Chem.* **2005**, 1247−1257.

(15) Schmidt, K.; Brovelli, S. et al.; in preparation.

(16) Brown, A.; Kemp, C. M.; Mason, S. F. *J. Chem. Soc. A* **1971**, 751−755.

(17) Vander Donckt, E.; Nasielski, J.; Greenleaf, J. R.; Birks, J. B. *Chem. Phys. Lett.* **1968**, *2*, 409−410.

(18) Vander Donckt, E.; Matagne, M.; Sapir, M. *Chem. Phys. Lett.* **1973**, *20*, 81−84.

(19) Birks, J. B.; Birch, D. J. S.; Cordemans, E.; Vander Donckt, E. *Chem. Phys. Lett.* **1976**, *43*, 33−36.

(20) Dierksen, M.; Grimme, S. *J. Chem. Phys.* **2004**, *120*, 3544−3554.

(21) Dierksen, M.; Grimme, S. *J. Phys. Chem. A* **2004**, *108*, 10225−10237.

(22) Minaev, B.; Ågren, H. *Chem. Phys.* **2005**, *305*, 215−239.

(23) Grellmann, K.-H.; Hentzschel, P.; Wismontski-Kittel, T.; Fischer, E. *J. Photochem.* **1979**, *11*, 197−213.

(24) Chen, P. *Unimolecular and Bimolecular Ion−Molecule Reaction Dynamics*; Wiley: New York, 1994.

(25) Runge, E.; Gross, E. K. U. *Phys. Rev. Lett.* **1984**, *52*, 997−1000.

(26) Gross, E. K. U.; Kohn, W. *Adv. Quantum Chem.* **1990**, *21*, 255−291.

(27) Gross, E. K. U.; Dobson, J. F.; Petersilka, M. *Top. Curr. Chem.* **1996**, *181*, 81−172.

(28) Becke, A. D. *J. Chem. Phys.* **1993**, *98*, 5648−5652.

(29) (a) Bauernschmitt, R.; Ahlrichs, R. *Chem. Phys. Lett.* **1996**, *256*, 454−464. (b) Bauernschmitt, R.; Ahlrichs, R. *Chem. Phys. Lett.* **1997**, *264*, 573−578. (c) Furche, F.; Ahlrichs, R. *J. Chem. Phys.* **2002**, *117*, 7433−7447; see for current version: www.turbomole.de.

(30) Dewar, M. J. S.; Zoebisch, E. G.; Healy, E. F.; Stewart, J. J. P. *J. Am. Chem. Soc.* **1985**, *107*, 3902−3909.

(31) AMPAC 8; Semichem, Inc.: Shawnee, KS, 1992−2004.

(32) Reimers, J. *J. Chem. Phys.* **2001**, *115*, 9103−9109.

(33) Wong, M. W. *Chem. Phys. Lett.* **1996**, *256*, 391−399.

(34) Brédas, J. L.; Beljonne, D.; Coropceanu, V.; Cornil, J. *Chem. Rev.* **2004**, *104*, 4971−5003.

(35) Malagoli, M.; Coropceanu, V.; da Silva Filho, D. A.; Brédas, J. L. *J. Chem. Phys.* **2004**, *120*, 7490−7496.

(36) Grimme, S.; Peyerimhoff, S. D. *Chem. Phys.* **1996**, *204*, 411−417.

(37) Kuroda, R. *J. Chem. Soc., Perkin Trans. 2* **1982**, 789−794.

(38) Sironi, A. Crystal Structure of 1-aza-H5, private communication, **2005**.

(39) Buss, V.; Kolster, K. *Chem. Phys.* **1996**, *203*, 309−316.